Finite Element Surrogate Model for Electric Machines with Revolving Field – Application to IPM Motors

Dan M. Ionel
A. O. Smith Corp.
12100 W. Park Place
Milwaukee, WI 53224-9512
Email:dionel@aosmith.com

Mircea Popescu
Motor Design Ltd.
4 Scotland Street
Ellesmere SY12 0EG, UK
Email: mircea.popescu@motor-design.com

***Abstract*—The model allows the ultra-fast simulation of the steady-state performance of synchronous machines and is particularly suitable for brushless motors with non-overlapping windings having coils concentrated around the teeth. Finite element analysis (FEA) is employed only for calculating the magnetic vector potential in the coils. For the example IPM motors presented, as little as one magnetostatic FE solution was used for fundamental flux linkage and average torque computation. Two FE solutions were employed for core flux density waveforms and power loss estimation. A minimum of three solutions is recommended for torque ripple, back emf and induced voltage. A substantial reduction of one to two orders of magnitude was achieved for the solving time as compared with detailed time-stepping FEA. The surrogate FE model can also be tuned for increased speed, comparable with that of magnetic equivalent circuit solvers. The general applicability of the model is discussed and recommendations are provided. Successful validation was performed against detailed FEA and experiments.**

***Index Terms* – Brushless (BL) permanent-magnet (PM) motor, AC synchronous machine, IPM motor drive, finite-element analysis (FEA), flux density waveform, back emf, core loss, iron loss, non-overlapping winding, concentrated coils.**

I. Introduction

Brushless permanent magnet (PM) motors controlled by sine-wave drives, also commonly referred to as synchronous PM motors, are the typical choice for the latest generation of high-efficiency electric motion systems [1]. In this class, the motor designs with interior permanent magnet (IPM) rotors are particularly attractive due to their electromagnetic, mechanical and manufacturability advantages [2].

Generally, the design optimization of IPM machines is challenging, as the closed-form analytic and equivalent magnetic circuit methods face issues in dealing with the typical heavy magnetic saturation and with significant geometrical details, such as the PM slots and rotor bridges. In this respect, improved methods have been developed for specific configurations, e.g. [3], [4]. On a more general basis, finite element analysis (FEA) could be a powerful tool for solving such problems, but its requirement for rather expensive computational resources and especially the long solving time are limiting factors for wider penetration in the engineering design environment.

To overcome the barriers, surrogate model optimization [5], was recently proposed for actuators by Encica *el al* [6] and for electric machines by Giurgea *et al.* [7]. According to such formulations, a simple analytical model is employed for the analysis of a very large number of candidate designs. The results are then mapped (correlated/fitted) with a reduced set of data provided by a few selected designs, which are simulated with a more precise model that is typically based on detailed FEA. To be effective in the industrial practice, such a system would require automatic data transfer between the model object description and the analytical and the FEA modules. As the transfer tasks are in principle possible with state of the art software, this opens the possibility of employing a simplified FE formulation even at the initial stage of fast estimation, which otherwise would be carried out by analytical models. This paper describes such an ultra-fast FE technique that provides a subset of results comparable in terms of precision with those delivered by substantially more time-consuming FEA. By extension of terminology, this simplified/reduced/substitute model will be referred to in the following as a surrogate finite-element model (SFE).

A simulation of a motor and electronic drive system should be based in principle on a coupled field and circuit model, as for example, the one described by Mohammed *et al.* [8]. Over the years, in order to reduce computational efforts, while still providing satisfactorily accurate estimation of electric machine performance, simplified models have been proposed by different authors. Examples of this type include, among others, the work of Demerdash and Hamilton [9], Williamson *et al.* [10], Miller *et al.* [11] and Knight and Zahn [12]. Recently, the authors have published an ultra-fast FE method for brushless PM motors that took advantage of the slot-pitch symmetry of the stator magnetic circuit and proved to be suitable especially for topologies with a relatively large number of teeth per pole and with distributed windings [13].

The present paper brings further contributions on the subject by proposing a model which fully exploits the symmetries of

the electric circuit and eliminates the assumption of a low harmonic content of armature mmf. The new model is generally applicable to the steady-state operation of synchronous machines and is particularly well suited for brushless PM motors with non-overlapping windings having coils concentrated around the teeth. Examples are provided for IPM motors, which are of particular interest as their analytical models are considered to be still open to debate and improvement.

The method employs the abc reference frame, therefore avoiding the theoretical limitations of the conventional dq formulations. A minimum set of magnetostatic problems is solved in order to identify an SFE model in terms of the harmonic content of the magnetic vector potential in the coil sides. The main motor performance is then estimated, including the induced voltage, the average torque and torque ripple, the flux density waveforms and core losses.

II. Electromagnetic Field Analysis

In brushless synchronous motors, the PM field together with the armature reaction, which is established by the currents flowing through the stator windings, produce a fundamental revolving field and a rich content of space harmonics. The time harmonics, generated by the PWM voltage supply are neglected in the following analysis and the currents are assumed to be purely sinusoidal, a hypothesis typically accepted in drive systems that employ state of the art motor and current controllers. The computational procedures are explained with reference to a 3-phase system, but they are generally applicable to any poly-phase synchronous machine with electromagnetic or PM excitation.

In such a balanced and symmetric system, the flux linkages due to the electromagnetic field from the motor cross-section through the red, R, yellow Y and blue, B, phases have the same harmonic content and an incremental phase shift of 120 electrical degrees:

$$\begin{aligned}\Psi_R(t) &= \sum_{\nu=1}^{\nu_M} k_{s\nu}\Psi_\nu \cos\left[\nu\omega t + \phi_\nu\right] \\ \Psi_Y(t) &= \sum_{\nu=1}^{\nu_M} k_{s\nu}\Psi_\nu \cos\left[\nu\left(\omega t - 120^o\right) + \phi_\nu\right] \\ \Psi_B(t) &= \sum_{\nu=1}^{\nu_M} k_{s\nu}\Psi_\nu \cos\left[\nu\left(\omega t + 120^o\right) + \phi_\nu\right]\end{aligned} \tag{1}$$

where ω is the fundamental pulsation, ϕ_ν is the initial phase and $k_{s\nu}$ is the skew factor of the harmonic ν. The flux linkage Fourier series include all the space harmonics up to the maximum order ν_M.

A comprehensive approach for modeling the electromagnetic field in an electric machine is based on the diffusion equation, which is solved coupled with the equations of the driving circuit [14]. Because relatively small steps are required in order to prevent numerical instabilities, substantial computational resources are required and a long solution time is expected. These major drawbacks limit the usage of this state of the art technique in the practical industrial design engineering.

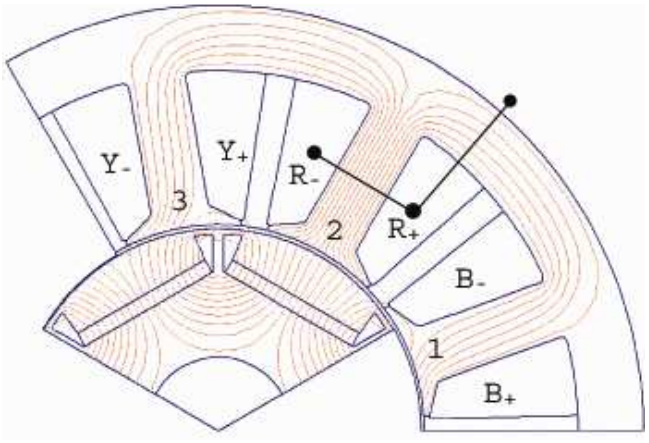

Fig. 1. FE computed flux distribution in the example 9-slot 6-pole IPM machine at open-circuit operation. Schematically shown are a coil placed around tooth 2 and a virtual coil placed around the back iron.

In synchronous IPMs the effect of eddy-currents is typically insignificant and can be neglected, making the simpler Poisson equation for the magnetic potential A [15],

$$\frac{\partial}{\partial x}\left(\frac{1}{\mu}\frac{\partial A}{\partial x}\right) + \frac{\partial}{\partial y}\left(\frac{1}{\mu}\frac{\partial A}{\partial y}\right) = -J - J_m \tag{2}$$

a suitable choice for modeling the steady-state operation at constant speed. In the previous 2D equation the current density J through the conductors is given and the PM equivalent current density J_m is defined by the known magnet remanence and permeability. The time variable t is transformed in a space variable,

$$\omega t = \theta = p\theta_r \tag{3}$$

namely the rotor position θ, which is measured in elec. deg. and linked to the mechanical position θ_r through the number of motor pole pairs, p. Using this approach, the machine operation is simulated through a number of successive snapshots, i.e. magnetostatic field problems. The field sources are represented by the PMs and the instantaneous distribution of stator currents, which is determined based on the rotor position and the electronic controller current set-point and torque angle.

For computational efficiency, (1) is solved only on the smallest possible domain, which is represented by a pole pair for the 9-slot 6-pole example shown in Fig.1 and considered in the following. The IPM prototype rotor employs high energy NdFeB magnets. The prototype stator has non-overlapping windings with concentrated coils wound around each tooth. Because of its topology with only three coils in the computational domain, each of the coils belonging to a different phase, this example provides a very good basis for introducing the computational algorithm. However, the method can be extended to a wider class of motors with non-overlapping or even with distributed windings.

The previous theory represents the basis of the simple – surrogate FE (SFE) based model. The rotor position and the

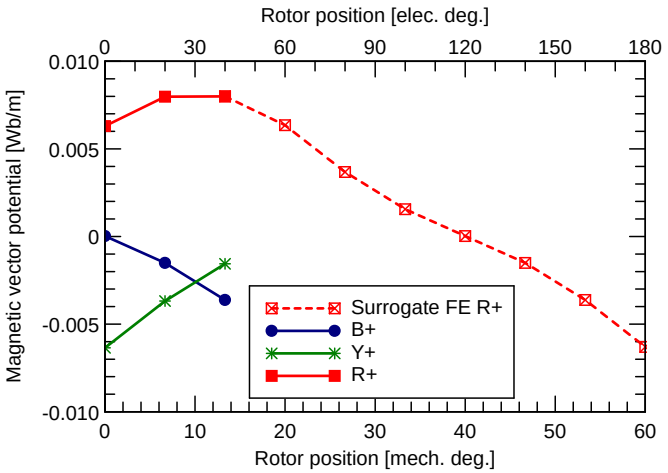

Fig. 2. Magnetic vector potential in the go (+) coil sides. Discrete points of the red R phase waveform are calculated using (5) and data from the other two phases.

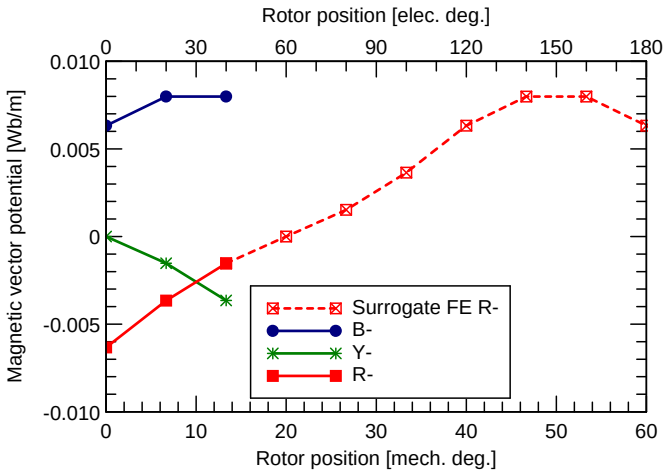

Fig. 3. Magnetic vector potential in the return (-) coil sides. Estimation over half electric cycle is performed from only 3 rotor positions covering 60 elec. degrees.

stator currents are input data and the magnetic vector potential in the go $(+)$ coils, $R+$, $Y+$, $B+$, and in the return $(-)$ coil sides, $R-$, $Y-$, $B-$, are the basic results that enable further post-processing. For example, the radial flux per unit of axial length through tooth 2 and through one turn of the coil placed around this tooth, is estimated from the average magnetic vector potential in the coil sides as

$$\Phi_{R+R-} = A_{R+} - A_{R-} \tag{4}$$

Based on (1), (3)–(4) and taking into account the symmetry of the electromagnetic circuit, the magnetic vector potential in the go $(+)$ coil side of the R phase can be calculated from the corresponding values in the other two phases:

$$\begin{aligned} A_{R+}(\theta + 60^\circ) &= -A_{Y+}(\theta) \\ A_{R+}(\theta + 120^\circ) &= A_{B+}(\theta)\ . \end{aligned} \tag{5}$$

Similar equations are available for the return $(-)$ coil sides.

The procedure for computing the phase flux linkage is exemplified with reference to Figs.1–4. Three magnetostatic FE simulations were performed with the rotor positioned as shown in Fig.1 at 0 deg. and at 6.67 and 13.33 mech. deg in the counter clockwise direction. The 3 solutions cover equidistantly 60 elec. deg., which represents the stator winding phase belt. Using the previous equations, a total of 9 points were made available for estimating the magnetic vector potential in the coil sides of phase R (Figs. 2-3).

Using these waveforms, the flux linkage per turn is calculated with (4) and, by multiplication with the number of series turns per phase, the flux linkage per unit of axial length is computed. In Fig.4, the discrete points between 180 and 360 elec. deg. were calculated using the half-wave symmetry condition. As a result, 19 wave points and 18 sample intervals were made available from only 3 FE magnetostatic problems. With the least computational effort, when only one FEA is performed in the initial rotor position, 7 equidistant points can be estimated on the waveform. As it can be

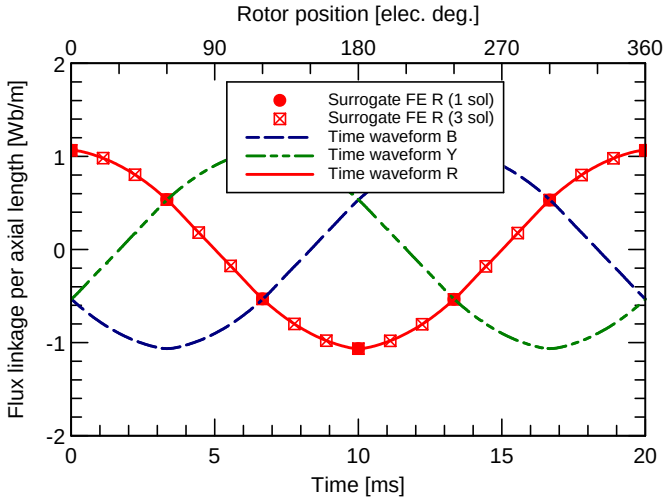

Fig. 4. Flux linkage waveforms for open-circuit operation. The 19 data points, available from an SFE based on 3 magnetostatic FE solutions, overlap the 7 data points of an SFE identified from a single magnetostatic FE.

observed, the discrete points are situated on the waveforms calculated with the same mesh and a time-domain FEA with 360 steps per electric cycle, which required substantially more computational effort.

In the example motor of Fig.1, the flux density is substantially radial in the tooth and predominantly circumferential (tangential) in the back-iron (yoke). In fact, this type of field distribution is typical for designs with small number of slots per pole and non-overlapping windings with concentrated coils as well as, in general, for high-polarity brushless PM motors.

For a first-approach engineering analysis, the flux density in tooth B_{th} and yoke B_{yk} can be therefore estimated as:

$$B_{th} = \frac{\Phi_{R+R-}}{t_w} = \frac{A_{R+} - A_{R-}}{t_w} \tag{6}$$

$$B_{yk} = \frac{A_{R+} - 0}{y_w} = \frac{A_{R+}}{y_w} \tag{7}$$

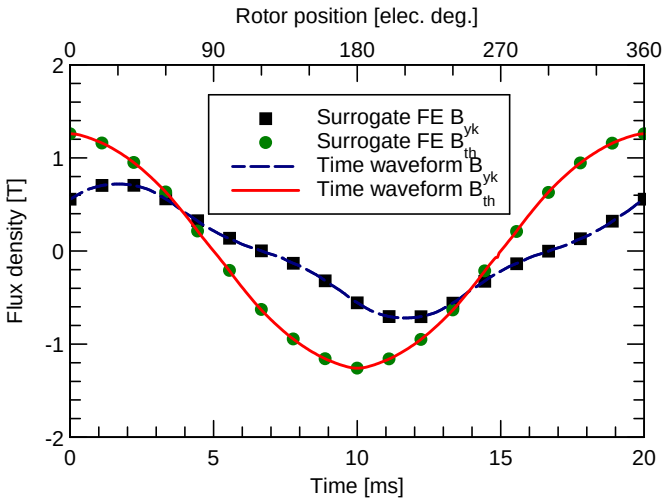

Fig. 5. Open-circuit flux density waveforms in the mid tooth and center yoke above the slot for the example of Fig.1.

where t_w and y_w are the tooth and yoke width, respectively. Equation (7) can be intuitively explained on the basis of a virtual coil placed around the back iron as shown in Fig.1 and the assumption of zero magnetic field outside the motor.

For the example open-circuit study, when no currents are flowing in the stator windings, the results are in line with those obtained by detailed and computationally expensive time-stepping FEA (Fig. 5). In principle, a more precise computation, which minimizes the effect of slot leakage, can be performed by employing in (6) and (7) the magnetic vector potential values in points situated closer to the teeth and yoke, rather than the average value of the magnetic vector potential in the coil sides.

Using this procedure, the flux density in the tooth is basically a scaling of the flux linkage through the coil surrounding the tooth and the two waveforms have the same typical quasi-sinusoidal shape. On the other hand, the flux density in the yoke, which is a scaling of the magnetic vector potential in the adjacent coil-side, has a richer harmonic content as it will be later discussed.

III. Machine Performance Simulation - Numerical and Experimental Validation

The most suitable validation for the surrogate FE (SFE) model previously described was provided by a detailed time-stepping FEA performed with the same geometry, mesh and material models, which ensured a fair basis of comparison. Experimental data was also used, where available, and all of the examples indicate satisfactory agreement between measurements and calculations.

In order to minimize the harmonic effects, the rotor of the prototype motor was built with two identical axial modules, which were assembled staggered by one quarter of stator slot pitch, achieving a one-step approximation of a half-slot pitch continuous skew. The 2D computed waveforms were then post-processed employing the method described in [16]. As

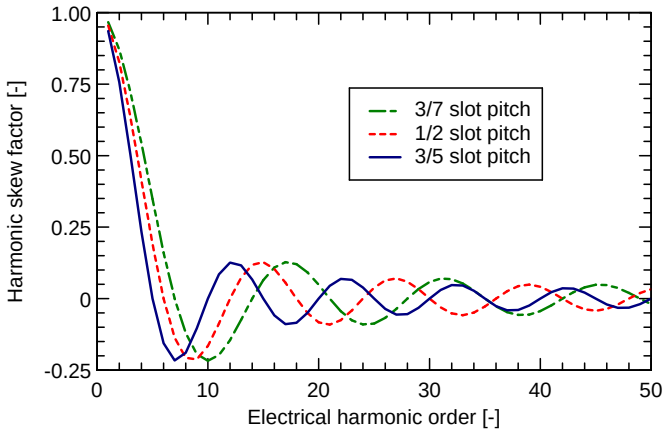

Fig. 6. Parametric study for the harmonic skew factor. The prototype motor of Fig.1 incorporates an equivalent skew of half stator slot pitch.

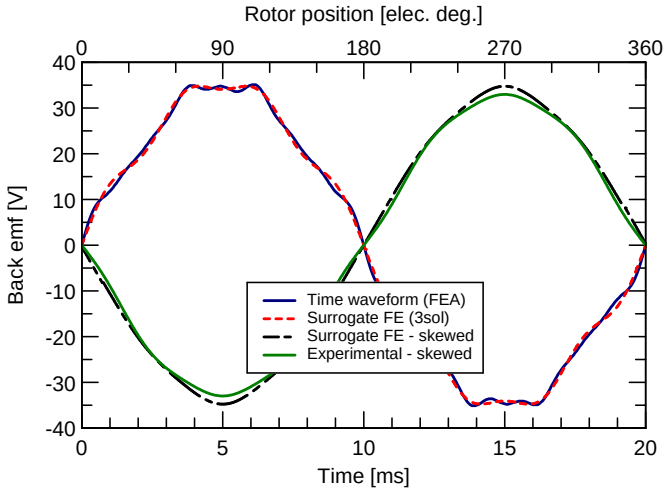

Fig. 7. Computed and measured back emf waveforms at 1,000rpm for the example motor of Fig.1. For clarity, two of the waveforms are plotted in anti-phase.

exemplified in (1), the surrogate SFE model is also able to take into account a continuous skew through the harmonic factor

$$k_{s\nu} = \frac{2}{\nu\beta} \cdot \sin\left(\frac{\nu\beta}{2}\right) \tag{8}$$

where the skew angle β is measured in elec. radians. The graph of Fig. 6 illustrates the half-slot skew as a good compromise for reducing both the 5th and the 7th harmonic, which are expected to be significant. At the same time, the skew is drastically affecting the higher order harmonics.

The back emf waveform of Fig. 7 was computed from the SFE model by differentiation of the flux linkage

$$e_R = -\frac{d\Psi}{d\theta} \cdot \frac{d\theta}{dt} = \omega \sum_{\nu=1}^{\nu_M} k_{s\nu} \nu \Psi_\nu \sin\left(\nu\theta + \phi_\nu\right) \tag{9}$$

This equation clearly illustrates how even the smallest values of flux linkage harmonics are amplified in the back emf waveform through multiplication with the harmonic number.

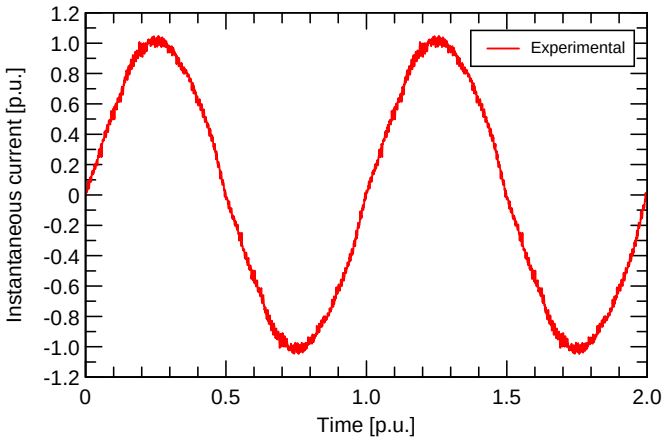

Fig. 8. Typical experimental waveform of phase current electronically regulated at high switching frequency. In the computations the currents are assumed to be perfectly sinusoidal.

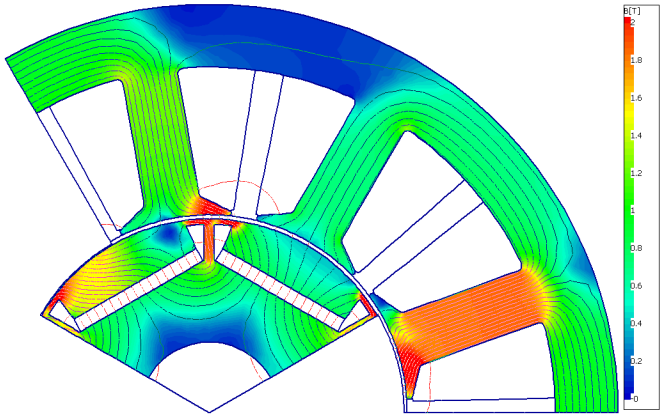

Fig. 9. Flux lines and density plots of the magnetic field in the cross-section of the 9-slot 6-pole IPM motor example operating at rated current and a torque angle of 110 deg.

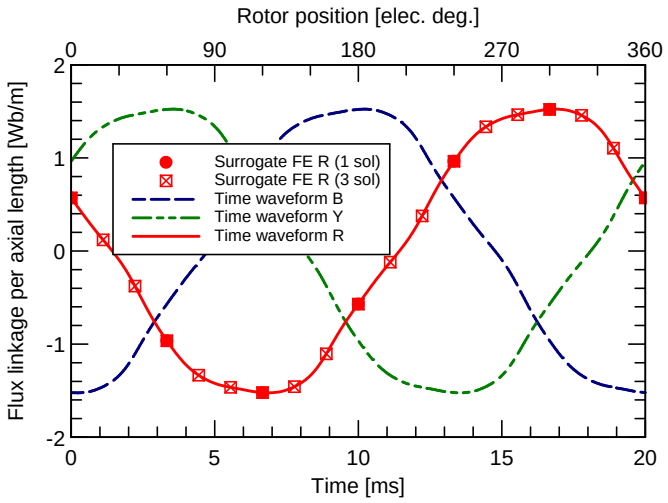

Fig. 10. Flux linkage waveforms for on-load operation. The 19 data points, available from an SFE based on 3 magnetostatic FE solutions, overlap the 7 data points of an SFE identified from a single magnetostatic FE.

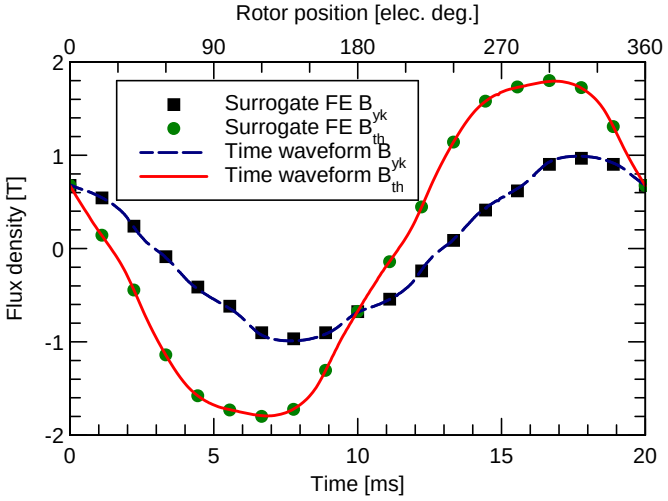

Fig. 11. Flux density waveforms in the mid tooth and center yoke above the slot for the example motor of Fig. 9. The discrete data points of the SFE model are used for Fourier analysis.

In the SFE model, as well as in the time-stepping FEA to which is compared, the on-load phase currents are considered to be purely sinusoidal. Generally, this is an acceptable assumption in systems employing adequately designed motors and suitably tuned current regulators (Fig. 8). Load studies were performed with the magnetic circuit non-linearly saturated, as illustrated by the flux plot of Fig. 9. Under these conditions, the flux linkage (Fig. 10) and the flux density (Fig. 11) are heavily distorted. The rich harmonic content of the armature reaction is contributing to these results.

The induced phase voltage can be computed in the SFE model on the basis of the flux linkage in the motor cross-section, similarly to (9), and by considering also the contributions due to the winding resistance and end-winding leakage inductance. Through the incorporation of the skew effect, the distortions from the computed waveform were greatly reduced and good agreement was achieved over a wide range of loads with the measured fundamental voltage of the PWM supply voltage (Fig. 12).

Using the values of the flux density in the tooth and yoke (see Figs. 5 and 11), the specific power loss per unit of mass in the stator core is determined as the sum of a hysteresis

$$w_h = \sum_{\nu=1}^{\nu_M} k_{h\nu}\left(\nu f_1, B_\nu\right) \cdot \left(\nu f_1\right) \cdot B_\nu^2 \qquad (10)$$

and an eddy current component

$$w_e = \sum_{\nu=1}^{\nu_M} k_{e\nu}\left(\nu f_1, B_\nu\right) \cdot \left(\nu f_1\right)^2 \cdot B_\nu^2 \ , \qquad (11)$$

where the core loss coefficients are dependent of harmonic frequency νf_1 and peak value of flux density B_ν [17]. The Fourier analysis implies the super-position principle, under the assumption that the main contribution is due to the fundamental frequency f_1, which corresponds to the pulsation ω. At load, the core losses are also affected by a correction factor, which accounts for the PWM harmonics [18].

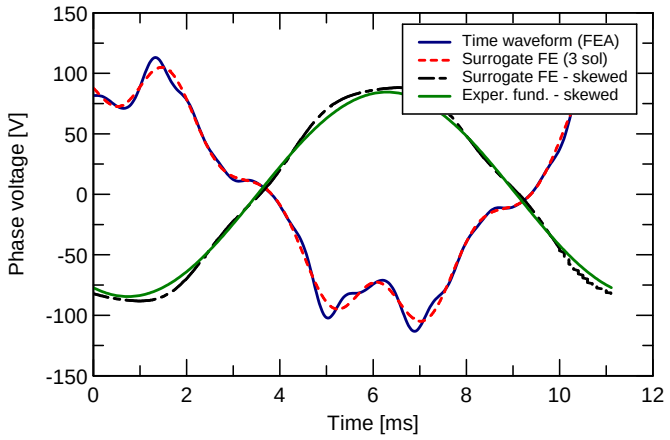

Fig. 12. Computed and measured phase voltage in the example motor of Fig.9 operating on-load at 1,800rpm. For clarity, two of the waveforms are plotted in anti-phase.

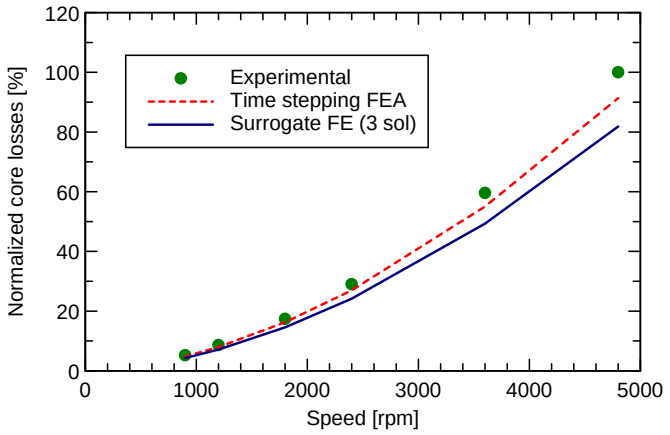

Fig. 13. Core losses vs. speed for the example motor operating at rated load current.

The prediction of the core losses with the SFE model is affected by the assumptions of unidirectional magnetic field, i.e. only radial component in the tooth and tangential in the back-iron, as well as by the relatively low resolution both in space and time. Improvements could be achieved, in principle, either through an approximate and systematic adjustment in order to align results with those from a more precise model, or by combining the SFE model with another technique, such as for example the ultra-fast space-time transformation method previously proposed by the authors [13]. However, even without any adjustment, the results for the studied example were overall satisfactory as shown in Fig. 13.

Because the SFE model incorporates at least a limited number of harmonics, it is possible to estimate the electromagnetic torque

$$T_e = p\left(i_R\frac{d\Psi_R}{d\theta} + i_Y\frac{d\Psi_Y}{d\theta} + i_B\frac{d\Psi_B}{d\theta}\right) \qquad (12)$$

and obtain an average value as well a ripple. Under the assumption of ideally sinusoidal currents, the torque will include harmonics ν_T, which together with flux linkage harmonics ν_Ψ

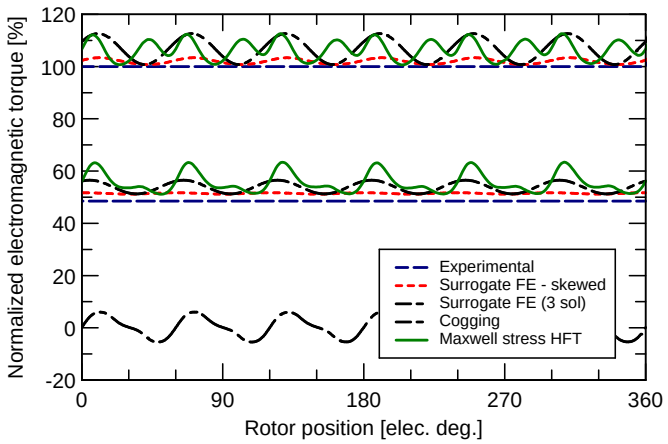

Fig. 14. Normalized electromagnetic torque at rated current and half rated current. The cogging torque is also shown.

TABLE I
OPEN-CIRCUIT CORE LOSSES IN THE EXAMPLE 18-SLOT 12-POLE IPM MACHINE WITH SPOKE ROTOR.

Speed	Time-stepping FEA	Surrogate FE 3 solutions	Experiment
[rpm]	[W]	[W]	[W]
1000	11.7	10.5	11.0
2000	39.1	37.1	38.0
3000	79.2	77.5	78.5

satisfy the relation $\nu_T = \nu_\Psi + 1$. For the example motor, the SFE model identified from 3 magnetostatic solutions includes flux harmonics up to the 7th order and the electromagnetic torque waveforms of Fig. 14 calculated with (12) include a 6th order ripple.

For the example 9-slot 6-pole motor at rated load, the peak to peak variation of this torque ripple is comparable with the one computed by time-stepping FEA in conjunction with a very precise method based on the Maxwell stress tensor [19]. Nevertheless, in this case the frequency of the ripple is different in between the two methods. The simulations with half rated current have better agreement for the frequency of ripple and poorer in terms of ripple magnitude. This example torque study, as well as others that are not included due to space limitations, provided interesting insights, which are subject to on-going investigations and anticipated to be covered in a future paper. The results of the model that includes the effect of skew, which reduces the ripple as well as the fundamental flux linkage and the average torque, compared satisfactorily with the experimental values that were derived based on low speed measurements of shaft torque and losses.

The model was validated also on other motors, some of which had a substantial higher harmonic content than the 9-slot 6-pole example previously studied. This is the case for an 18-slot 12-pole IPM prototype with a spoke rotor (Fig. 15) for which satisfactory results are reported in Fig. 16 for the back emf and in Table I for core losses.

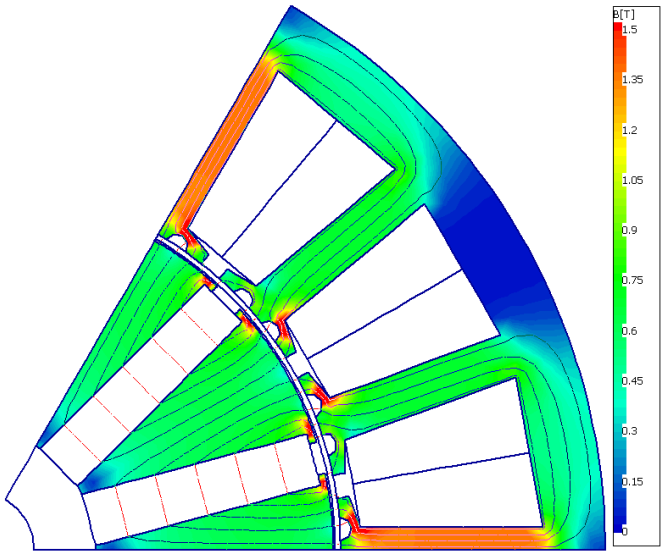

Fig. 15. Flux plot for the open-circuit operation of an 18-slot 12-pole example machine with concentrated coils and spoke IPM rotor with ferrite magnets.

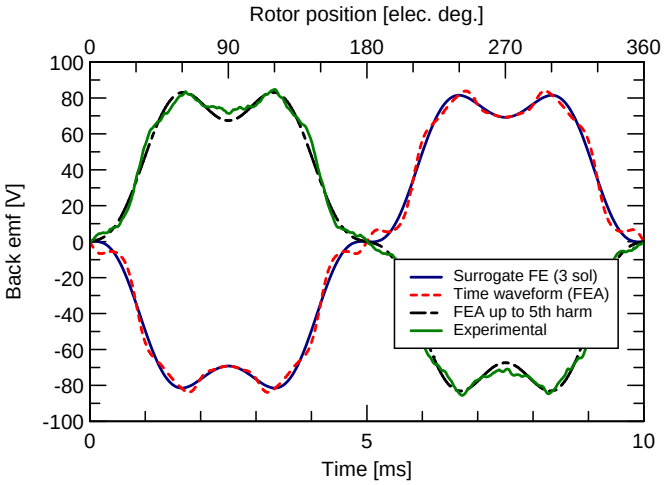

Fig. 16. Computed and measured back emf waveforms at 1,000rpm for the example motor of Fig. 15. For clarity, two of the waveforms are plotted in anti-phase.

IV. Discussion

A. Trading speed versus precision

The computational speed and the precision of the surrogate SFE model are largely influenced by the number of magnetostatic FE solutions employed. Each magnetostatic problem provides one value of magnetic vector potential per coil side and hence only one value of flux linkage per coil/phase. Making full use of the 3-phase electric circuit symmetry, 3 values of the per-phase flux linkage can be derived following the procedure previously described with reference to Figs. 2-4. Furthermore, making use of the half-wave anti-symmetry, 2 times more discrete points, hence a total of 6 values of flux data can be estimated. Finally, the waveform value at 360 deg. is equal to the one at 0 deg. providing one additional data point. The relation between the number of FE magnetostatic solutions, s, sampling intervals and maximum order of the harmonics ν_M that can be calculated by Fourier analysis is exemplified and summarized in Table II.

TABLE II
Relations specific to the surrogate SFE model.

Magnetostatic FE solutions	Waveform points	Sampling intervals	Maximum harmonic order ν_M
1	7	6	2
2	13	12	5
3	19	18	8
4	25	24	11
5	31	30	14
s	$6s+1$	$6s$	$3s-1$

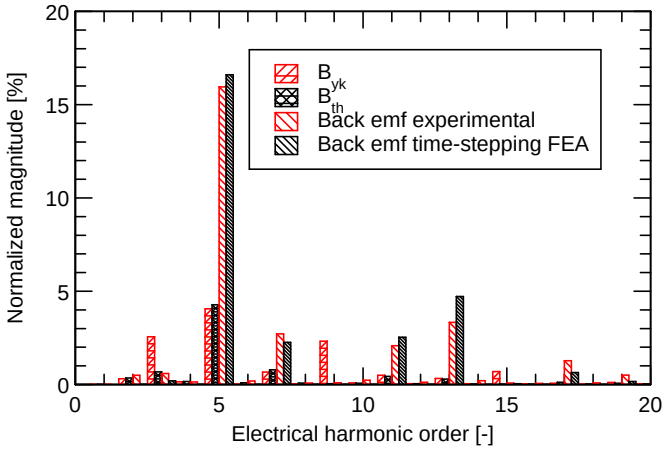

Fig. 17. Harmonic spectrum analysis for two different problems: the flux density of Fig. 11 and the back emf of Fig. 16. The amplitude values are normalized to the respective fundamental, which is omitted from the plot.

In practical problems, the choice of s is driven by the maximum harmonic order of interest for the analysis. For example, the back emf of the previous 18-slot 12-pole spoke IPM motor example has a significant 13th harmonic, as illustrated in Fig. 17. Therefore, according to Table II at least 5 magnetostatic FE solutions should be employed, although the visual inspection of the results plotted in Fig. 16 would indicate that as few as 3 solutions may be enough. For the on-load flux density study in the core of the 9-slot 6-pole example motor (Fig. 11), according to the harmonic analysis results of Fig. 17, in principle, as few as 2 magnetostatic FE problems should be enough. This is because in this case there are no significant harmonics (i.e. with a normalized magnitude larger than 1%) above the 5th.

Nevertheless, special caution is recommended when the harmonic of interest has an order substantially close to the maximum available from the Fourier analysis. This is particularly valid for studies with very low number of FE solutions. For example, although the results of average torque listed in the last column of Table III, which were computed with (12) based on a single FE solution, are very good, in such cases, small variations in the conditions, e.g. the non-linear change in local saturation with rotor position, may cause estimate perturbations. It should be noted that these last column results were calculated in the reference position of Fig. 1, which

TABLE III
TORQUE AND TORQUE RIPPLE VERSUS TORQUE ANGLE AT RATED CURRENT FOR THE EXAMPLE MOTOR OF FIG. 9.

Torque angle	Time-stepping FEA		Surrogate FE 3 FE solutions		Surrogate FE 1 FE solution
[elec. deg.]	Avg. [p.u.]	Ripple [%]	Avg. [p.u.]	Ripple [%]	Avg. [pu] [p.u.]
90	0.82	13.5	0.85	12.6	0.84
100	0.90	11.1	0.92	12.0	0.93
110	0.97	11.3	0.97	11.1	1.00
120	1.00	13.1	0.98	10.7	1.02
130	0.98	15.0	0.95	12.2	1.01
140	0.87	20.0	0.85	16.0	0.92
150	0.70	28.5	0.70	28.7	0.77
160	0.48	52.7	0.50	27.1	0.56
170	0.25	117.6	0.28	48.2	0.31
180	0.00	N/A	0.01	N/A	0.05

yields zero cogging as shown in Fig. 14.

With further reference to the results of Table III, the average torque computed with an SFE based on only 3 magnetostatic solutions compares favorably with the results of a time-domain FEA that required two orders of magnitude more solving time. For this particular example, the same holds true for the values of the ripple torque, which are out of line only at relatively large torque angles when the typical operation involves a very high harmonic content. The average torque is reported in a per unit system with reference to the maximum value calculated by detailed FEA at 120 deg. torque angle. The ripple torque is defined as a percentage of the torque at the particular operating point and hence is meaningless at 180 deg. torque angle, which yields theoretically zero torque.

In principle, there are no general rules for establishing the maximum order of harmonics to be studied and hence the number of FE magnetostatic solutions. For the open-circuit operation the choice is somewhat simpler, for a given stator topology a main determining factor being the equivalent IPM pole arc. Things are more complicated for load simulations, when the proportion of armature reaction to PM field, the magnetic saturation and the mmf harmonics may all be important. Practical experience may help, but when in doubt it is advisable to choose a relatively high and therefore safer value for s. After all, with state of the art software and hardware a small number of additional magnetostatic FE simulations will only require a few extra seconds or less.

Additional savings of computational resources can be achieved with SFE by adequate meshing. Because only the magnetic vector potential is of interest from the FE solution, in principle (very) coarse meshes can be employed yielding a reduced number of equations, even comparable with that employed in the latest generation of magnetic equivalent circuit (MEC) solvers. Typically, the computational time is proportional with the number of FE nodes (unknowns) squared and therefore approximately halving the mesh density may reduce solving time by one order of magnitude. The coarse mesh example of Fig. 18, which has less than 1,000 nodes, achieved this objective, while the maximum errors noted in the average magnetic potential in the coil side were below 3% as compared with those provided by a somewhat refined mesh, which was used throughout the reported studies.

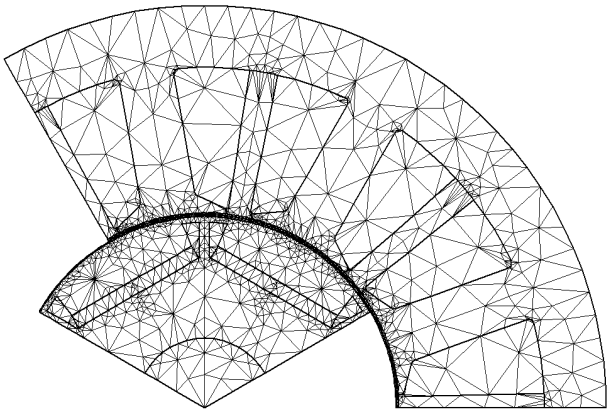

Fig. 18. The SFE model can employ very coarse meshes reducing the computational effort towards the level specific to magnetic equivalent circuit (MEC) models.

B. The flux linkage vs. current diagram and the surrogate SFE

A couple of other minimum-effort schemes have been proposed lately for computing the average torque of a brushless PM motor driven with sine-wave currents. One of them is based on a variation of the Maxwell stress [19] and can be used in conjunction with the SFE model previously described. The other method employs $d-q$ analysis and an approximation of the per phase flux linkage vs. current diagram [11].

Example diagrams are provided in Fig. 19 for the 9-slot 6-pole motor studied. The average torque can be estimated based on the area of the substantially elliptically-shaped cycle [20]. The 7 data points of flux linkage calculated from a single magnetostatic solution should not be used to draw a polygon that would erroneously estimate average torque, as shown in Fig.19. Instead, this reduced set of points, or the 19 data points available from 3 magnetostatic solutions, should be employed to calculate the fundamental flux linkage waveform and based on this to estimate the area of the ellipse. At the same time, if present, the effect of the stator to rotor relative axial skew can also be incorporated in the Fourier harmonic analysis.

The advantages of the new SFE model over the previously published work [11], [19], include a minimum-effort concurrent estimation of the torque ripple and induced voltage waveform. Additionally, the waveforms of flux density in the teeth and back iron are computed and based on these the core losses are estimated.

V. CONCLUSION

The surrogate FE (SFE) model described is suitable for the steady-state simulation of a wide class of synchronous machines with electromagnetic and PM excitation. The model was introduced on example IPM motors with non-overlapping windings and concentrated coils around the stator teeth. Satisfactory validation was demonstrated against results provided by more laborious time-stepping FEA and experimental data. The procedure, which is based on the values of the magnetic

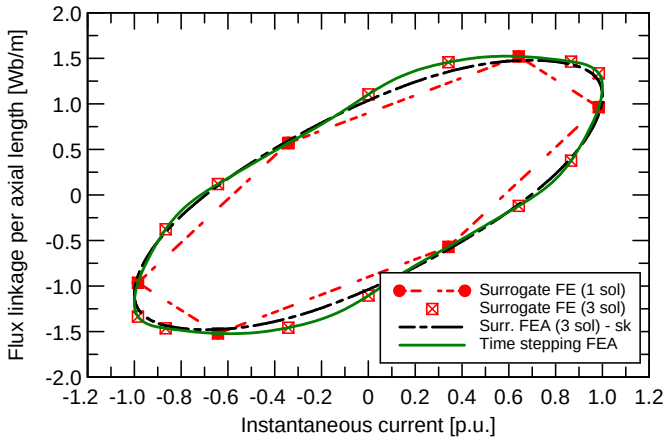

Fig. 19. Example flux linkage vs. current diagrams. A Fourier series, rather than discrete points, was employed for flux linkage and yielded satisfactory results even from a single magnetostatic FE analysis.

vector potential in the coil sides, can be extended and applied for any concentrated or distributed winding patterns.

The SFE could be classified as an intermediate step between analytical methods and detailed FEA. By employing a coarse FE mesh and by studying a reduced number of harmonics, requiring only a very small number of magnetostatic FE solutions, the solution time for the SFE can be reduced almost to a level comparable with that of a magnetic equivalent circuit (MEC) solver. Alternatively, the model can be tuned for improved precision. In such an arrangement, for the studied examples, the model was able to deliver comparable results with time-domain FEA, while the solving time was reduced by one to two orders of magnitude.

The examples presented, which are relevant for typical electromagnetic loading and design topologies, also indicate that as little as one magnetostatic FE solution maybe enough for average torque estimation. On the other hand, only two FE solutions maybe needed for core flux density waveforms and power loss estimation. A minimum of three magnetostatic solutions is recommended for torque ripple, back emf and induced voltage.

Because only the magnetic vector potential in the coil sides is required from the FEA, the SFE model is considered to be suitable for implementation at the user level of commercially available software. Multi-dimensional look-up tables of flux linkage and of flux density versus current and torque angle can be derived for use with system simulators for estimating motor performance, including the core losses, which are typically a major component in IPM motors. As such, the model has the potential of providing the practicing engineer with a useful tool for all the stages of an optimal design process.

Acknowledgment

The authors are thankful for the suggestions of their colleagues from A.O. Smith Corp., Mrs. Janice Fitzgerald and Mr. Ron Bartos.

References

[1] I. Boldea and S. Nasar, *Electric Drives (2nd ed.)*. Boca Raton, FL: Taylor & Francis (CRC Press), 2005.

[2] D. M. Ionel, "Ipm motors: A new solution for high-performance appliances," *Appliance Mag.*, vol. 65, no. 11, pp. 22–25, Nov. 2008.

[3] J. R. Hendershot and T. J. E. Miller, *Design of Brushless Permanent-Magnet Motors*. Mentor, OH and Oxford, UK: Magna Physics and Oxford University Press, 1994.

[4] E. C. Lovelace, T. M. Jahns, and J. Lang, "A saturating lumped-parameter model for an interior pm synchronous machine," *IEEE Trans. on IAS*, vol. 38, no. 3, pp. 645–650, May/June 2002.

[5] J. Bandler, Q. Cheng, S. Dakroury, A. Mohamed, M. Bakr, K. Madsen, and J. Sondergaard, "Space mapping: the state of the art," *Microwave Theory and Techniques, IEEE Transactions on*, vol. 52, no. 1, pp. 337–361, Jan. 2004.

[6] L. Encica, J. Paulides, E. Lomonova, and A. Vandenput, "Electromagnetic and thermal design of a linear actuator using output polynomial space mapping," *Industry Applications, IEEE Transactions on*, vol. 44, no. 2, pp. 534–542, March-April 2008.

[7] S. Giurgea, D. Fodorean, G. Cirrincione, A. Miraoui, and M. Cirrincione, "Multimodel optimization based on the response surface of the reduced fem simulation model with application to a pmsm," *Magnetics, IEEE Transactions on*, vol. 44, no. 9, pp. 2153–2157, Sept. 2008.

[8] O. A. Mohammed, S. Liu, and Z. Liu, "Physical modeling of pm synchronous motors for integrated coupling with machine drives," *IEEE Trans. on MAG*, vol. 41, no. 5, pp. 1628–1631, May 2005.

[9] N. Demerdash and H. Hamilton, "Effect of rotor asymmetry on field forms and eddy current losses in stator conductors due to radial flux," *IEEE Trans. on PAS*, vol. PAS-103, no. 7, pp. 1999–2004, 1972.

[10] S. Williamson, L. Lim, and M. Robinson, "Finite-element models for cage induction motor analysis," *IEEE Trans. on IAS*, vol. 26, no. 6, pp. 1007–1017, Nov/Dec 1990.

[11] T. Miller, M. Popescu, C. Cossar, M. McGilp, M. Olaru, A. Davies, J. Sturgess, and A. Sitzia, "Embedded finite-element solver for computation of brushless permanent-magnet motors," *Industry Applications, IEEE Transactions on*, vol. 44, no. 4, pp. 1124–1133, July-Aug. 2008.

[12] A. Knight and Y. Zhan, "Identification of flux density harmonics and resulting iron losses in induction machines with nonsinusoidal supplies," *Magnetics, IEEE Transactions on*, vol. 44, no. 6, pp. 1562–1565, June 2008.

[13] D. M. Ionel and M. Popescu, "Ultra-fast finite element analysis of brushless pm machines based on space-time transformations," in *Electric Machines and Drives Conference, 2009. IEMDC '09. IEEE International*, May 2009, pp. 521–528.

[14] S. Salon, *Finite element analysis of electrical machines*. Boston, USA: Kluwer Academic Publisher, 1995.

[15] N. Bianchi, *Electrical Machine Analysis Using Finite Elements*. Boca Raton, FL: CRC Press, 2005.

[16] J. Eastham, D. Ionel, M. Balchin, T. Betzer, and E. Demeter, "Finite element analysis of an interior-magnet brushless dc machine, with a step-skewed rotor," *Magnetics, IEEE Transactions on*, vol. 33, no. 2, pp. 2117–2119, Mar 1997.

[17] D. M. Ionel, M. Popescu, M. I. McGilp, T. J. E. Miller, S. J. Dellinger, and R. J. Heideman, "Computation of core losses in electrical machines using improved models for laminated steel," *IEEE Trans. on IAS*, vol. 43, no. 6, pp. 1554–1564, Nov/Dec 2007.

[18] D. Ionel, M. Popescu, C. Cossar, M. McGilp, A. Boglietti, and A. Cavagnino, "A general model of the laminated steel losses in electric motors with pwm voltage supply," in *Industry Applications Society Annual Meeting, 2008. IAS '08. IEEE*, Oct. 2008, pp. 1–7.

[19] D. M. Ionel, M. Popescu, M. I. McGilp, T. J. E. Miller, and S. J. Dellinger, "Assessment of torque components in brushless permanent-magnet machines through numerical analysis of the electromagnetic field," *IEEE Trans. on IAS*, vol. 41, no. 5, pp. 1149–1158, Sept/Oct 2005.

[20] D. Staton, R. Deodhar, W. Soong, and T. Miller, "Torque prediction using the flux-mmf diagram in ac, dc, and reluctance motors," *Industry Applications, IEEE Transactions on*, vol. 32, no. 1, pp. 180–188, Jan/Feb 1996.